On the Use of Non-uniform RIS and Parasitic Strips to Improve Antenna CP Performance

Qi Zheng[1,2*], Chenjiang Guo[1], Jun Ding[1], Guy A. E. Vandenbosch[2]

[1] School of Electronics and Information, Northwestern Polytechnical University, Xi'an China,
[2] ESAT-TELEMIC Research Division, Department of Electrical Engineering, KU Leuven, Leuven, Belgium.
[*] zhq930908@mail.nwpu.edu.cn

Abstract: The effect of using a non-uniform reactive impedance surface (RIS) on the circular polarisation (CP) performance of a planar antenna is investigated. It is shown that a very wide axial ratio (AR) bandwidth can be obtained, especially when the RIS is combined with parasitic strips. This result is only possible thanks to the fact that the RIS is non-uniform. The technique is demonstrated by designing, building, and measuring a prototype. The simulated impedance bandwidth ($|S11| \leq -10$ dB) is 43.6% (4.3-6.7 GHz), and the simulated 3-dB AR bandwidth is 37.2% (4.6-6.7 GHz). The gain variation over the 3-dB AR bandwidth is 3-5.9 dBi. The experimental results are in good agreement with the simulations, validating the new concept.

1. Introduction

Circularly polarised (CP) antennas have been extensively used in satellite systems and wireless communications due to their robustness against polarisation rotations. CP microstrip antennas have attracted much attention because of their compact size, light weight, and low cost. In order to excite two orthogonal modes with 90° phase difference for obtaining CP radiation, different feeding techniques have been developed [1]. Among these techniques, the single-feed technique is the simplest one. Single-feed CP compact antennas are typically achieved by truncating corners of a square patch radiator [2], making slots or slits [3], or feeding a patch diagonally [4]. All these techniques suffer from a narrow impedance and axial ratio (AR) bandwidth. To solve this drawback, numerous techniques have been proposed, for example the use of parasitic elements [5-8].

Recently, metasurfaces (MSs) have been shown to offer the ability to further miniaturize antenna size and improve radiation performance [9-13]. Such MSs are reactive impedance surfaces (RIS) [14-19], high-impedance surfaces (HIS) [20] [21] and artificial magnetic conductor (AMC) [22] [23], both based on periodic metallic patches on top of a grounded dielectric substrate. However, these publications are mainly focusing on linearly polarised (LP) antennas.

In order to obtain CP radiation with RIS, two techniques can be used. The first technique is to integrate a RIS layer under a CP driven patch radiator. The RIS unit cell is square and is chosen to obtain a reflection phase of 0° at the operating frequency. In [24], a triple-band circularly polarised GPS antenna is proposed using stacked patches over a RIS for enhancing antenna radiation efficiency. Several single-feed CP microstrip antennas with asymmetric/symmetric slots/slits on an RIS have been studied in detail [25][26]. However, all these designs suffer from a narrow bandwidth. In [27], a novel circular-ring slotted rectangular patch with 7×7 unit cells is proposed to provide a 28.3% 3-dB AR bandwidth. In [28], an H-shaped patch antenna with 4×4 square unit cells is presented to achieve a 27.5% 3-dB AR bandwidth. It can be concluded that for the first technique the main challenge is to obtain a wide band with the designed patch radiator.

The second technique is to employ a diagonally fed CP patch antenna over an RIS. At the operating frequency, the reflection phases of the RIS structure with rectangular unit cell are chosen as +90° or –90° for *x*- and *y*- polarisation, respectively. In [29], a 45° diagonally fed corner-truncated square patch antenna on an artificial ground shows a wide 3-dB AR bandwidth of 20.4%. The main challenge for this technique is to combine the transmitted wave from the antenna and the reflected wave from the structure in such a way that circular polarisation is obtained.

Characteristic mode (CM) theory is an excellent tool to physically explain the working mechanisms of antennas [30-33]. It provides insight into electromagnetic resonances of current distributions. Recently, CM analysis has been widely used in the design and optimization of metamaterial-based slot antennas [34-37].

In this paper, the effect of using a non-uniform RIS on the CP performance of a planar antenna is investigated. It is proven that a very wide AR bandwidth can be obtained by combining the RIS with parasitic strips. The non-uniformity of the RIS is crucial. The new concept is illustrated by making a design starting from a typical corner-truncated square patch antenna. As far as the authors can see, it is the first time that the non-uniform RIS topology is used to improve the CP performance of a planar antenna. Up to now non-uniform MSs have been investigated only to improve LP antenna bandwidth [38], [39] and aperture efficiency [40].

The paper is organized as follows. Section 2 gives the CM theory analysis of a typical CP patch antenna and two RIS-based CP antennas. Section 3 presents a wideband CP patch antenna with parasitic strips over a non-uniform RIS. Section 4 gives the measured impedance matching and radiation properties. Section 5 concludes the paper.

2. Circularly polarised microstrip patch antenna using non-uniform RIS

In this section, first the excited modes of a typical CP patch antenna, a uniform RIS and a non-uniform RIS are revealed by using CM analysis. Then the uniform RIS and the non-uniform RIS are integrated within the CP patch antenna for wide impedance matching and CP characteristics. A

comparison is made between the uniform and the non-uniform RISs.

2.1. CM analysis for a typical CP antenna

Fig. 1 shows a typical classical design of a single-feed CP patch antenna [1]. The antenna consists of a corner-truncated square patch printed on top of a single-layer FR-4 substrate ($\varepsilon_r = 4.3$ and $\tan\delta = 0.02$), which is a low-cost and commonly used material [7, 19, 21, 22]. The antenna is fed by a coaxial probe at the location $(0, -l_f)$ with respect to the center of the antenna.

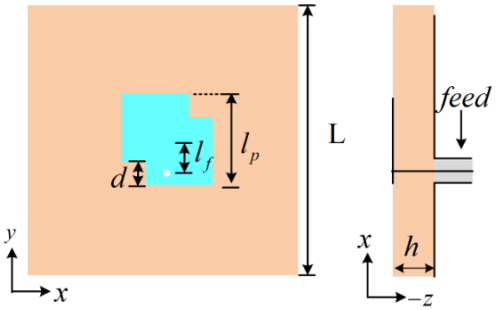

(a) (b)

Fig. 1. *Schemetic view of a single-feed CP microstrip antenna,* $l_f = 4\,mm$, $l_p = 9.5\,mm$, $d = 3.7\,mm$, $h = 3.5\,mm$, $L = 34\,mm$.

(a) *top view,* ***(b)*** *side view.*

In CM theory, the modal significance MS [30] ($MS_n = 1/|1 + j\lambda_n|$) and mode angle [31] ($\alpha_n = 180° - \tan^{-1}(\lambda_n)$) of the eigenvalue λ_n of a characteristic current mode *n* can be calculated. These two parameters are independent of the excitation or source. By using a proper feeding technique, an antenna can be forced to operate in a specific mode. Note that this method is general and can thus also be used for metamaterial-based antennas [34-37].

A CM analysis is carried out for the corner-truncated patch in the frequency range of 4-8 GHz. Fig. 2 gives the simulated MS and characteristic angle obtained with CST Microwave Studio Suite 2017. The substrate is set as loss-free for simulation, which at this moment is a fundamental requirement to be able to work with characteristic modes in commercial solvers. It is found that modes 1 and 2 present an equal MS and a phase difference of 120° at 7.18 GHz. The corresponding modal currents ***J₁*** and ***J₂*** at 7.18 GHz are displayed in Fig. 3. The black arrow represents the main direction of a model current. Since ***J₁*** and ***J₂*** have equal amplitudes and are orthogonal to each other, they have the potential to be combined to get CP radiation near 7.18 GHz.

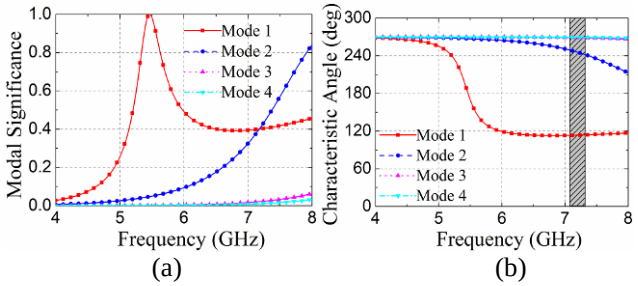

(a) (b)

Fig 2. *MS and characteristic angle of the corner-truncated patch antenna*

(a) *MS,* ***(b)*** *characteristic angle.*

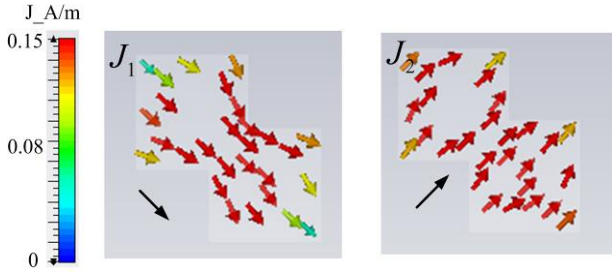

Fig 3 *Modal currents at 7.18 GHz*

2.2. CM analysis of uniform and non-uniform RIS structure

In order to extend the bandwidth of the CP patch antenna, a uniform RIS is used. The RIS is implemented in between two FR-4 substrates ($\varepsilon_r = 4.3$ and $\tan\delta = 0.02$) with thicknesses h_1 and h_2, respectively. The unit cell of the RIS was designed in HFSS with appropriate PEC and PMC boundaries to mimic the periodicity, see Fig. 4(a). The unit cell has size *p* and contains a single square patch with size *a*. A TEM incident wave excites the structure. The phase of the reflected wave in terms of the patch size *a* is depicted in Fig. 4(b). It can be seen that the size *a* has a great influence on the reflection characteristics. With the increasing of *a*, the reflection phase curve shifts to lower frequencies. At a patch size of 6 mm, a 0° reflection phase occurs at 5.4 GHz and the band of reflection phases in the range ±90° is from 4.5 GHz to 6.2 GHz, providing a wide inductive region.

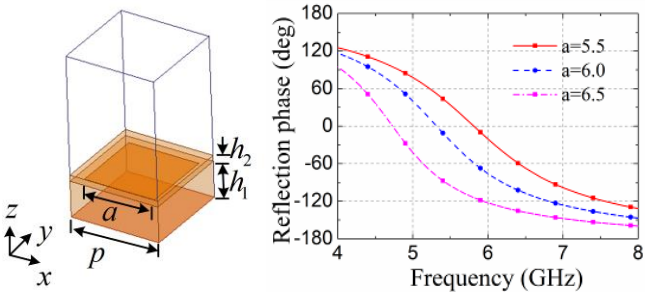

(a) (b)

Fig 4. *Simulation results of RIS,* $p = 7.5\,mm$, $h_1 = 3\,mm$, $h_2 = 0.5\,mm$

(a) *unit cell of RIS,* ***(b)*** *reflection phase of RIS,*

The RIS-structure provides additional resonances and coupling effects with the patch are involved. Here, first the number of uniform unit cells was optimized. It was verified that 4×4 uniform RIS units offer the best CP radiation performance under the corner-truncated patch. On the basis of the RIS with uniform unit cells, a non-uniform structure is proposed to enlarge the AR bandwidth. In contrast with previous studies [21], [25], [29] where the RIS unit cell was designed based on an infinite periodic lattice, CM theory is employed here to analyse and optimise the structure, explicitly taking into account the finite substrate and the finite number of RIS unit cells. This is done by studying the modal currents as a function of both the frequency and the dimensions of the patches.

Fig. 5(a) illustrates a classical uniform RIS structure consisting of 4×4 square patches. The unit cell has a patch

size a_0 with a period p. More flexibility is obtained by also considering non-uniform RIS structures, see Fig. 5(b). The non-uniform structure consists of 4×4 square patches with two patch sizes of a_1 and a_1 and with a fixed period p. Then, a CM analysis is carried out on the uniform and non-uniform RIS structures.

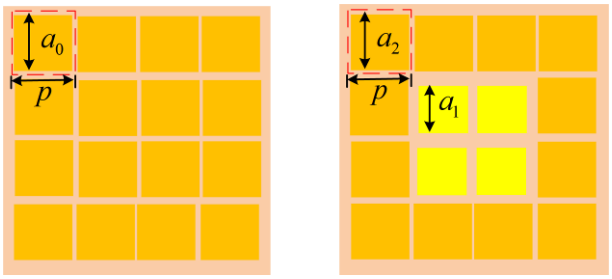

(a) (b)

Fig 5. *Two types of RIS structures,* $p=7.5$ mm, $a_0=6$ mm, $a_1=5.5$ mm, $a_2=6.5$ mm
(a) *uniform RIS,* ***(b)*** *non-uniform RIS*

The MS of the first 4 characteristic modes of the uniform RIS and the optimized non-uniform RIS are displayed in Fig. 6(a) and (b), respectively. According to Fig. 6(a), it can be concluded that Mode 1 (***J₁***) and Mode 2 (***J₂***) are modes with nearly the same MS and with the same resonant frequency of 6.74 GHz. The other two modes (***J₃*** and ***J₄***) show a similar tendency of variation and also have the same resonant frequency. According to Fig. 6(b), similar results are obtained for the non-uniform RIS. The first 2 modes (Mode 1 and Mode 2) resonate at 6.44 GHz and share nearly the same MS. The other two modes, Mode 3 and Mode 4, have a similar variation tendency and have the same resonant frequency.

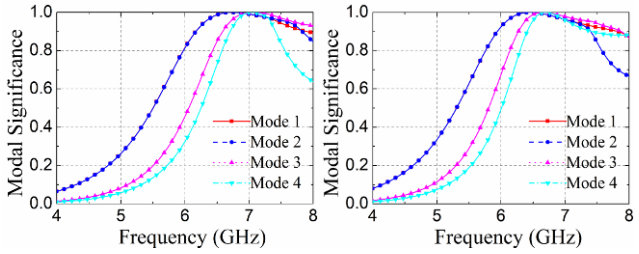

(a) (b)

Fig 6. *MSs of the RISs*
(a) uniform RIS, **(b)** non-uniform RIS

Fig. 7 gives the characteristic modal currents in the two structures. For the uniform RIS in Fig. 7(a), it can be seen that at 6.74 GHz the two dominant modes ***J₁*** and ***J₂*** are a pair of orthogonal modes in the *x*- and *y*-direction, respectively. The currents of these two dominant modes are mainly generated on the center four patches. By adjusting both the x and y sizes of these center patches, the amplitudes and phases of these (modal) currents can be tuned, in such a way that the two dominant modes at 6.44 GHz become a pair of orthogonal modes in the two diagonal directions, respectively, as shown in Fig. 7(b). This means that now the dominant modes of the non-uniform RIS are similar to those of the driven patch radiator.

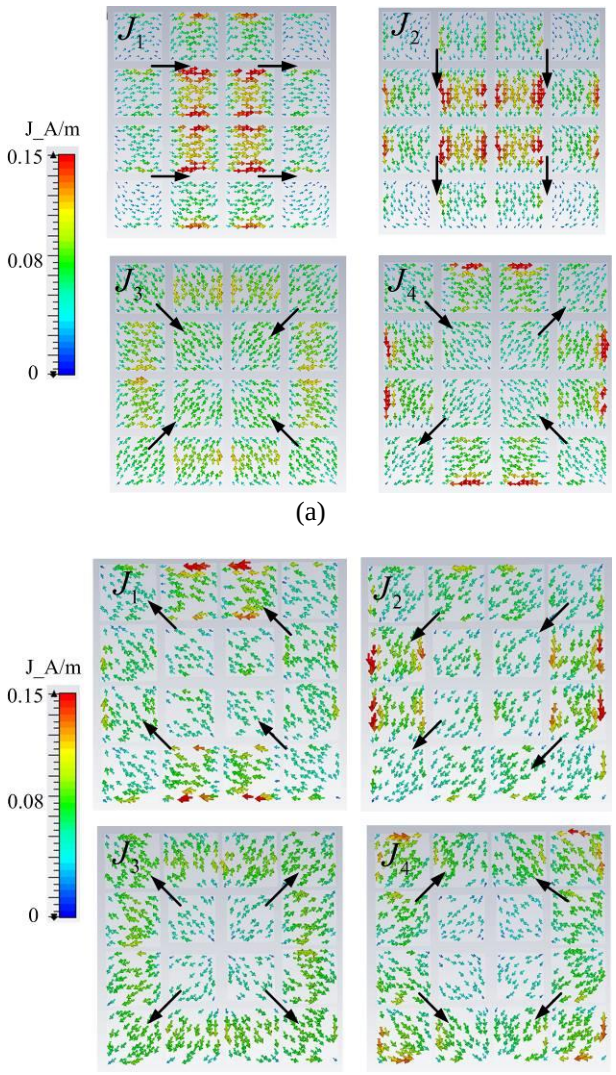

Fig 7. *Modal currents in the RISs*
(a) *uniform RIS at 6.74 GHz,* ***(b)*** *the non-uniform RIS at 6.44 GHz*

2.3. CP Antennas over uniform and non-uniform RIS structures

In this section the CP antenna is combined both with the uniform and the non-uniform RIS, see Fig. 8. The RIS structures are the same as in Fig. 5. The antenna is kept the same as in Fig. 1.

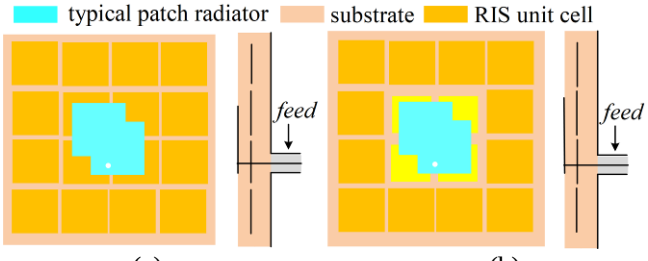

(a) (b)

Fig 8. Schemetic view of two antennas over the RISs
(a) *uniform RIS,* ***(b)*** *non-uniform RIS*

Fig. 9(a) gives the impedance bandwidths of the corner-truncated patch antenna (Ant. 1), the patch antenna over the

uniform RIS (Ant. 2) and the patch antenna over the non-uniform RIS (Ant. 3). It can be seen that the impedance bandwidth is significantly enhanced by the introduction of the RIS structures. Fig. 9(b) depicts the AR bandwidth of the three antennas. It is viewed that Ant. 1 has one minimum AR point (above 3 dB) at 6.9 GHz. Ant. 2 has two minimum AR points, one below and one above 3 dB. Ant. 3 has a 3-dB AR bandwidth of 4.95-6.35 GHz and two minimum AR points occurring at 5.1 GHz and 6.1 GHz, respectively. The second minimum AR point of the uniform RIS-based Ant. 2 shifts to lower frequencies when using non-uniform RIS, which results in a drastic axial ratio improvement. Thanks to the non-uniformity of the RIS, the CP characteristics are thus considerably improved. The operational frequency of the traditional corner-truncated square patch is shifted to the lower frequency region, which means a miniaturization is obtained [17], [18].

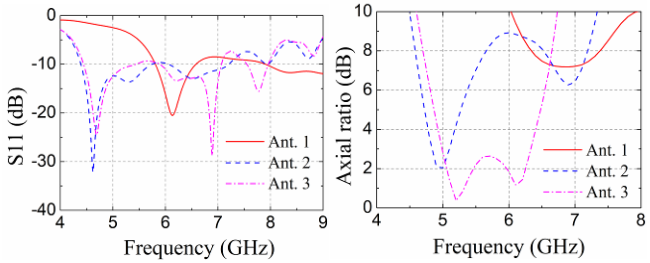

(a) (b)

Fig 9*. Simulated results of Ant.1, Ant.2, and Ant.3.*
(a) *S11,* ***(b)*** *AR*

Fig. 10(a) shows the side view of the uniform RIS. Fig. 10(b) shows the equivalent π-network circuit model between two adjacent unit cells, according to the transmission line model of [22]. The capacitances in this model can be used to make a first estimate of the patch length. The conductances model the losses and the radiation. For a single patch located at a height h_1 above a grounded substrate, the capacititance is

$$C_s = \frac{\varepsilon_0}{2}(-0.636\ln(k_0 h_1)) \quad (1)$$

with k_0 the wavenumber and ε_0 the vacuum permittivity [41]. The equivalent capacitance of a microstrip-gap-discontinuity with a gap distance s is given by

$$C_{eq}^0 = \frac{\varepsilon}{2\pi}[\ln 2 + \ln(\frac{A}{A-1} + \sqrt{\frac{A+1}{A-1}})] \quad (2)$$

with $A = \cosh(s\pi/2h_1)$ [42].

The initial patch size is assumed as half the value of effective wavelength ($\lambda_{eff}/2$). The actual physical length of the patch is shorter by a factor C_{eq}^0/C_s due to the higher capacitance caused by the gap, which can be approximate given by

$$L_{\text{patch}} = \frac{(\lambda_{eff}/2)}{C_{eq}^0/C_s} \quad (3)$$

with λ_{eff} the effective wavelength.

For a single patch antenna, its resonant frequency is reached when the patch is approximately half the effective wavelength ($\lambda_{eff}/2$). In the uniform RIS, C_{eq}^0 will affect this relation. These approximate expressions (1) and (2) allow to assess the reseonant frequency in relation to the physical configuration, namely substrate permittivity, thickness, patch length, and gap distance. For example, increasing the substrate permittivity decreases the resonant frequency; increasing the patch length decreases the resonant frequency, etc. Compared with the uniform RIS, the non-uniform RIS provides more freedom to adjust the equivalent capacitances. This is key in broadening the bandwidth of the non-uniform RIS-based CP antenna, for example by simply adjusting the patch sizes.

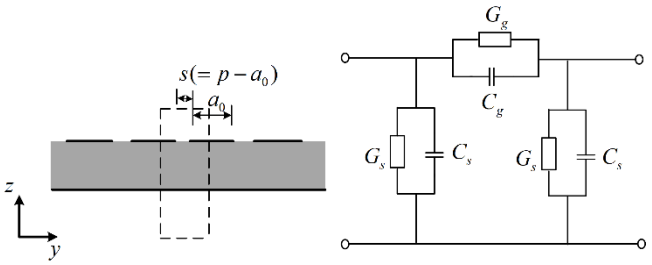

Fig. 10 *Transmission line model of uniform RIS*
(a) side view
(b) equivalent circuit model

3. CP microstrip antenna with parasitic strips over non-uniform RIS

In this section, the widening of the AR bandwidth is taken even further by combining the non-uniform RIS with parasitic strips.

3.1. Bandwidth enhancement with parasitic elements

In this section a pair of parasitic strips is loaded on the top layer to enlarge the 3-dB AR bandwidth. Fig. 11 shows the configuration (Ant. 4). The distance between the corner-truncated square patch and each parasitic strip is sd. Each strip has two arms with width sw and with lengths sl_1 and sl_2, respectively. An optimization was carried out to obtain a maximum impedance bandwidth from 4.3 GHz to 6.7 GHz and a maximum 3-dB AR bandwidth from 4.6 GHz to 6.7 GHz for this structure. The resulting parameters are: $l_f = 4$ mm, $l_p = 9.5$ mm, $d = 4.2$ mm, $h_1 = 3$ mm, $h_2 = 0.5$ mm, $L = 34$ mm, $p = 7.5$ mm, $a_1 = 5.5$ mm, $a_2 = 6.5$ mm, $sl_1 = 11$ mm, $sl_2 = 4$ mm, $sd = 0.3$ mm, $sw = 1$ mm. The simulated S11 and AR are given in Fig. 12. Comparing with Ant. 3, Ant. 4 has a wider 3-dB AR bandwidth.

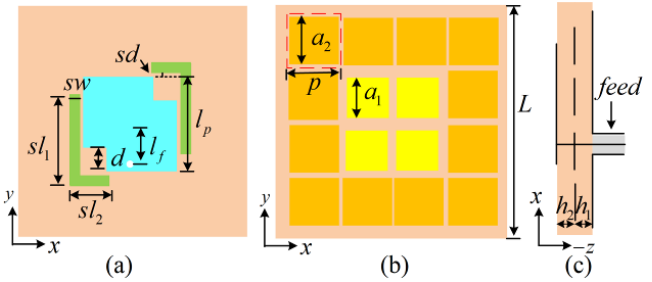

Fig.11 *Configuration of Ant. 4*
(a) *top view of corner-truncated patch with parasitic strips,* ***(b)*** *top view of non-uniform RIS,* ***(c)*** *side view.*

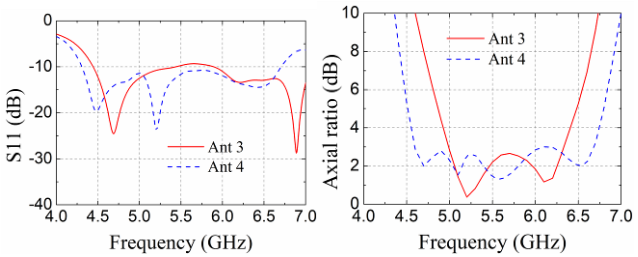

(a) (b)

Fig 12. *Simulated results of Ant. 3 and Ant. 4*
(a) *S11,* ***(b)*** *AR*

3.2. Effect of the sizes of the parasitic strips

In this section, a parametric study is carried out to understand the effect of the key parameters sl_1, sl_2, sd and sw of the strips on the CP radiation performance. The effects of dimensions sl_1 and sl_2 of the parasitic strips on the impedance matching and AR are shown in Fig. 13. As can be seen in Figs. 13(a) and (c), the impedance bandwidth changes only marginally, and the AR bandwidth shifts to lower frequencies. In can be seen in Figs. 13(b) and (d) that with the increase of sl_1 and sl_2, the AR values become lower in the upper part of the band but deteriorate in the lower part of the band.

The effects of dimensions sd and sw on the impedance matching and AR are shown in Fig. 14. With the increase of sd and sw, the impedance bandwidth and resonant frequencies keep nearly the same, and the AR values become lower in the lower part of the band but deteriorate in the upper part of the band.

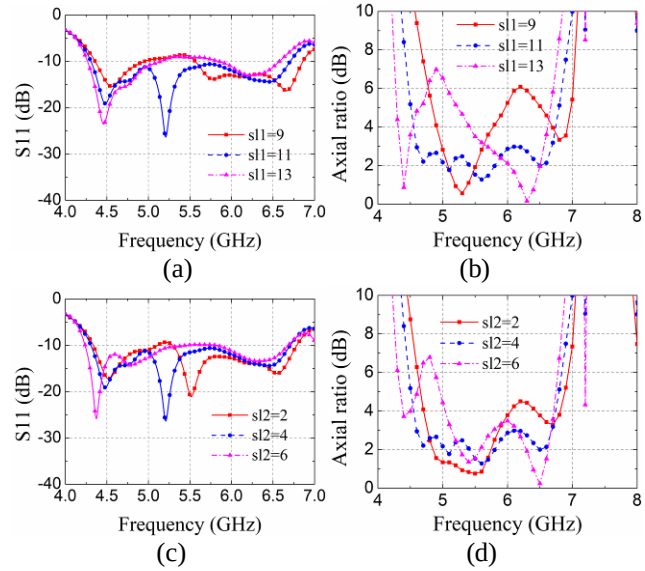

(a) (b)

(c) (d)

Fig 13. *S11 and AR for different parameters*
(a) *S11 with different* sl_1, ***(b)*** *AR with different* sl_1, ***(c)*** *S11 with different* sl_2, ***(d)*** *AR with different* sl_2

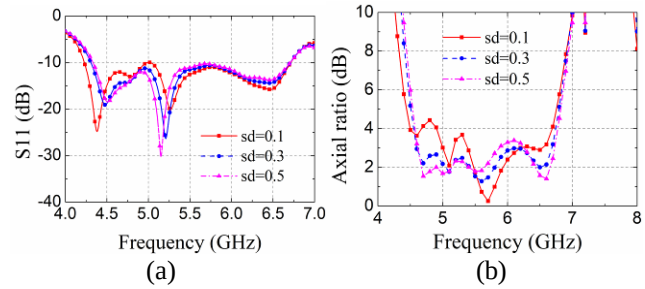

(a) (b)

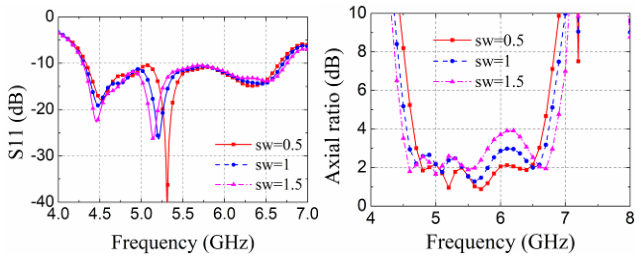

(c) (d)

Fig 14. *S11 and AR for different parameters*
(a) *S11 with different sd*, ***(b)*** *AR with different sd*, ***(c)*** *S11 with different sw*, ***(d)*** *AR with different sw*

In summary, the CP performance in the higher frequency region can be enhanced by increasing the lengths sl_1 and sl_2 and decreasing the distance sd and width sw. Inversely, the CP performance in the lower frequency region can be enhanced by decreasing the lengths sl_1 and sl_2 and increasing the distance sd and width sw. A wideband CP radiation can be obtained by optimizing these parameters.

To sum up, four antennas were designed/optimized in order to obtain an increasingly wideband CP operation around 5.5 GHz: a classical antenna (Ant. 1), the same topology extended with a RIS structure (Ant. 2), yielding two minimum AR points near 5.5 GHz with a higher AR bandwidth, a modified structure with a non-uniform RIS (Ant. 3), and the non-uniform RIS structure extended with two parasitic strips (Ant. 4). The comparison of the four antennas clearly proves the AR bandwidth widening capabilities of the non-uniform RIS, certainly when combined with parasitic strips.

4. Measurement and discussion

A prototype of the proposed antenna was fabricated and measured, as shown in Fig. 15. The overall dimensions are $34\times34\times3.5\ \text{mm}^3$ ($0.62\lambda_0\times0.62\lambda_0\times0.064\lambda_0$ at 5.5 GHz). Fig. 16(a) gives the measured and simulated S-parameters. The measured bandwidth is 4.48-6.75 GHz, and the simulated one is 4.3-6.7 GHz. There is only a slight frequency shift. Fig. 16(b) gives the measured 3-dB AR and total realized gain (broadside) including all field components in the boresight direction. The measured 3-dB AR bandwidth is 4.75-6.6 GHz, and the simulated one is 4.6-6.7 GHz. The measured gain varies from 4.0 to 7.0 dBic over the 3-dB AR bandwidth with a maximum gain of 7.0 dBic obtained at 4.9 GHz. The simulated peak gain of 5.9 dBic occurs at 4.8 GHz. A drop at 5.2 GHz occurs due to the drop of radiation efficiency. The measured and simulated results are in good agreement in the high frequency region. The discrepancies in the low frequency region are among others due to fabrication errors and the imperfect measurement environment. There is a big difference in the low band and a very small difference in the high band region. The possible reason is the fact that the dielectric constant of the substrates is not totally uniform. The gain at low frequencies is higher than the one at high frequencies, which is due to the loading of the parasitic element. The simulated radiation efficiency varies from 65% to 85% within the working band.

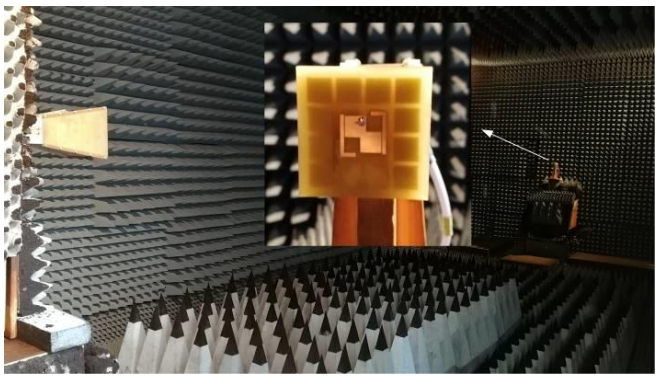

Fig. 15 *Fabricated prototype and measurement setup in the anechoic chamber*

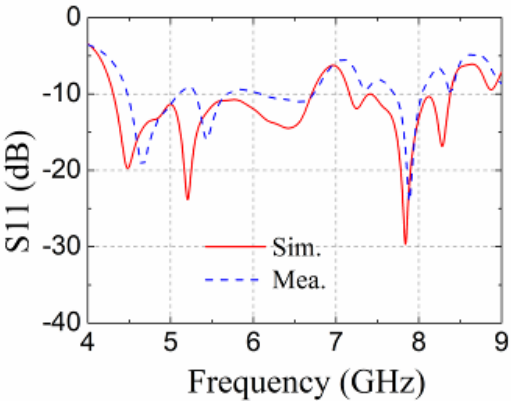

(a)

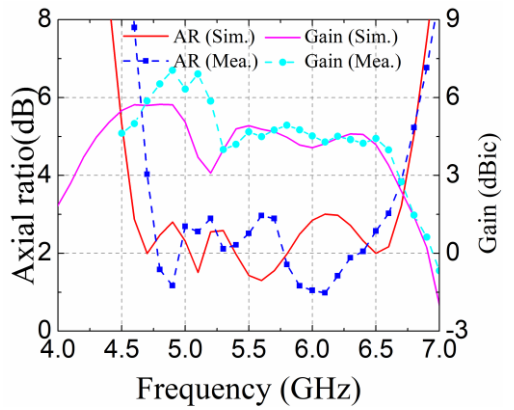

(b)

Fig. 16 *Simulated and measured results* ***(a)*** *S11,* ***(b)*** *AR and realized gain.*

The normalized radiation patterns at 4.7 GHz, 5.6 GHz and 6.6 GHz are plotted in Fig 17. It can be viewed that the measured and simulated co-polarised field components (RHCP) are in good agreement. The differences between the measured and simulated LHCP are mainly caused by imperfect measurement environment (VNA and environmental noise). The measured half-power beamwidths at 5.6 GHz are 77° and 88° in the *xoz*- and *yoz*-plane, respectively. Both the half-power beamwidths at the lower frequency 4.7 GHz and at the upper frequency 6.6 GHz are over 75° in the *xoz*- and *yoz*-planes. The slight beam offset was due to the off-axis feeding of the driven corner-truncated patch.

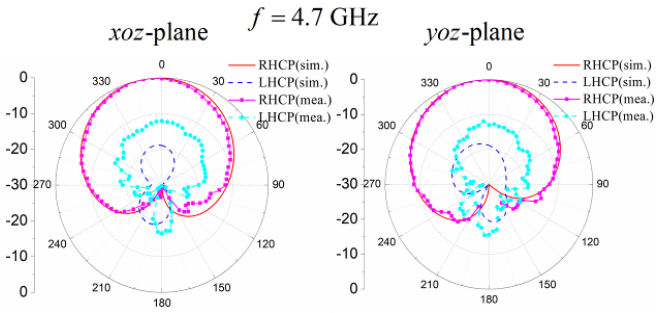

(a)

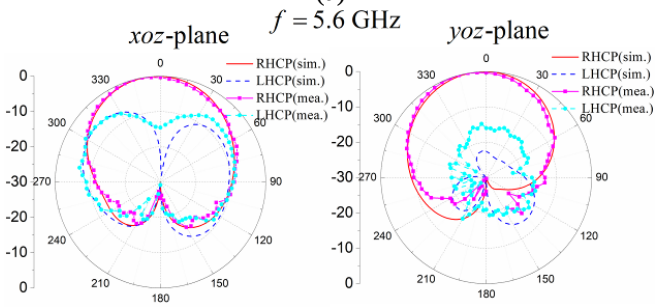

(b)

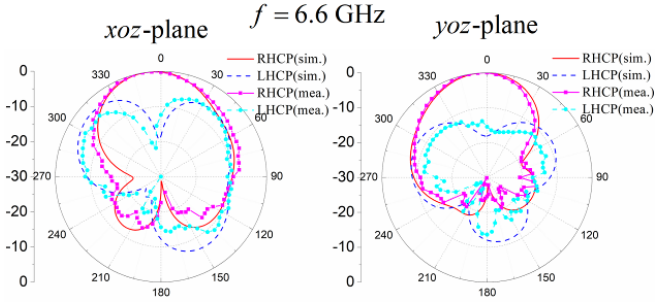

(c)

Fig. 17 *Radiation patterns* ***(a)*** *4.7 GHz,* ***(b)*** *5.6 GHz,* ***(c)*** *6.6 GHz*

A comparison between the proposed design and other antennas in literature is given in Table I. In order to have a fair comparison, only sufficiently thin (planar) antennas are considered. Compared with similar (uniform) RIS-based patch antennas [20-24], our antenna with the non-uniform RIS and parasitic strips yields the widest 3-dB AR bandwidth, illustrating the new concept of using the non-uniform RIS explicitly to improve CP characteristics. Compared with MS-based antennas [9] [30], the proposed antenna yields a wider 3-dB AR bandwidth.

Table I Comparison of other similar antennas in literature

Refs	Center frequency (GHz)	Impedance BW (GHz, %)	3-dB AR BW (GHz, %)	Peak Gain (dBic)	Size(λ_0^3)/ ε_r	Antenna structures
[7]	3.0	0.18/6.0%	0.1/3.3%	2.7	$0.5\times0.27\times0.016$ / $\varepsilon_r = 4.4$	Notched circular patch antenna, parasitic patches

[9]	5.5	2.78/45.6%	1.3/23.4%	7.6	$0.58\times0.58\times0.056$ / $\varepsilon_r = 3.38$	Corner-truncated patch antenna, MS-based superstrate
[25]	2.3	0.32/14	0.35/15.3	5.7	$0.77\times0.77\times0.06$ / $\varepsilon_{r1} = 10.2$, $\varepsilon_{r2} = 3.5$	Slotted patch, 45° -oriented RIS
[26]	2.7	0.178/6.68	0.07/2.69	4.31	$0.315\times0.315\times0.033$ / $\varepsilon_r = 4.2$	Corner-truncated patch antenna, RIS
[27]	4.0	1.44/36.0	1.13/28.3	7.4	$0.822\times1.18\times0.06$ / $\varepsilon_r = 4.3$	Circular-ring slotted patch antenna, RIS
[28]	5.5	2.66/44.5	1.45/27.5	7.2	$0.58\times0.58\times0.1$ / $\varepsilon_r = 3.8$	H-shaped patch antenna, RIS
[29]	6.0	2.78/48.6	1.3/20.4	6.60	$0.78\times0.80\times0.096$ / $\varepsilon_r = 2.2$	Corner-truncated patch antenna, RIS
[35]	5.5	2.13/38.8%	0.8/14.3%	9.4	$1.37\times1.37\times0.071$ / $\varepsilon_r = 3.38$	Slot antenna, MS-based superstrate
This work (Ant. 4 sim.) *(Ant.4 mea.)*	**5.5**	**2.4/43.6** *(2.27/40.43)*	**2.1/37.2** *(1.85/32.6)*	**5.9** *(7.0)*	$0.62\times0.62\times0.064$ / $\varepsilon_r = 4.3$	**Corner-truncated patch antenna, parasitic strips, non-uniform RIS**

5. Conclusion

In this paper, a simple method was developed to enhance the CP performance of a planar antenna: the use of a non-uniform RIS. Uniform and non-uniform RIS structures were compared, after optimizing with CM theory, to show the capabilities of the new technique. The largest AR bandwidth available in literature for thin planar antennas was obtained: 32.6 % for an antenna of only 0.064 wavelengths thick.

6. Acknowledgments

Authors thank the support from the China Scholarship Council (No. 201806290108) and Science Research Project of Gansu Province Higher Educational Institutions (No. 2019A-268).

7. References

[1] S. Gao, Q. Luo, and F. Zhu, “Circularly polarized antennas,” John Wiley & Sons, 2013.

[2] P. C. Sharma, and K. C. Gupta, “Analysis and optimized design of single feed circularly polarized microstrip antennas,” *IEEE Trans. Antennas Propagat.*, 1983, 31, (6), pp. 949-955.

[3] Nasimuddin, X. Qing, and Z. N. Chen, “Compact asymmetric-slit microstrip antennas for circular polarization,” *IEEE Trans. Antennas Propag.*, 2011, 59, (1), pp. 285–288.

[4] Z. N. Chen, and X. Qing, “Slotted microstrip antennas for circular polarization with compact size,” *IEEE Antennas Propagat. Mag.*, 2013, 55, (2), pp.124-137.

[5] R. Li, et al., “Investigation of circularly polarized loop antennas with a parasitic element for bandwidth enhancement,” *IEEE Trans. Antennas Propag.*, 2005, 53, (12), pp. 3930-3939.

[6] W. Yang, et al. “Single-fed low profile broadband circularly polarized stacked patch antenna,” *IEEE Trans. Antennas Propag.*, 2014, 62, 10, pp. 5406-5410.

[7] J. F. Lin and Q. X. Chu, “Enhancing bandwidth of CP microstrip antenna by using parasitic patches in annular sector shapes to control electric field components,” *IEEE Antennas Wireless Propag. Lett.*, 2018, 17, (5), pp. 924-927.

[8] Z. Zhao, Y. Li, M. Xue, L. Wang, Z. Tang, and Y. Yin, “Design of wideband circularly polarized crossed-dipole antenna using parasitic modified patches,” *IEEE Access.*, 2019, 7, pp. 75227-75235.

[9] S. X. Ta, and P. Ikmo, “Low-profile broadband circularly polarized patch antenna using metasurface,” *IEEE Trans. Antennas Propag.*, 2015, 63, (12), pp.5929-5934.

[10] Q. Chen, and H. Zhang, “Dual-patch polarization conversion metasurface-based wideband circular polarization slot antenna,” *IEEE Access*, 2018, 6, pp. 74772-74777.

[11] Babazadeh et al., "A circularly polarized metasurface antenna", IET Conference Proceedings, p. 333, 2018.

[12] S. Jagtap, et al., “A wideband microstrip array design using RIS and PRS layers,” *IEEE Antennas Wireless Propag. Lett.*, 2018, 17, (3), pp. 509-512.

[13] Q. Zheng, et al., “Dual-band metasurface-based CP low-profile patch antenna with parasitic elements,” *IET Microwaves, Antennas & Propagation*, 2019, 13, (13), pp. 2360-2364.

[14] Lee et al., "Low profile quad-beam circularly polarised antenna using transmissive metasurface." *IET Microwaves, Antennas & Propagation*, 2019, 13, (10), pp. 1690-1698.

[15] Chen et al., "Miniaturised wideband antenna with low profile based on dual-layer metasurface." *IET Microwaves, Antennas & Propagation*, 2020, 14, (6), pp. 498-504.

[16] K. Buell, et al., “Patch antenna over RIS substrate: a novel miniaturized wideband planar antenna design,” in Proc. IEEE Antennas Propag. Soc. Int. Symp., Columbus, OH, USA, June. 269–272, 2003.

[17] H. Mosallaei and K. Sarabandi, “Antenna miniaturization and bandwidth enhancement using a reactive impedance substrate,” *IEEE Trans. Antennas Propag.*, 2004, 52, (9), pp. 2403–2414.

[18] C. Ren, L. Bernard, and R. Sauleau, “Investigations and design of small-size printed antennas on a reactive impedance substrate,” In Proc. 4th Eur. Conf. Antennas Propag, pp.12-16, Apr. 2010.

[19] Y. Dong, H. Toyao, and T. Itoh, “Compact circularly-polarized patch antenna loaded with metamaterial structures,” IEEE Trans. Antennas Propag., 2011, 59, (11), pp. 4329-4333.

[20] C. R. Simovski, P. de Maagt, and I. V. Melchakova, “High-impedance surfaces having stable resonance with respect to polarization and incidence angle,” *IEEE Trans. Antennas Propag.*, 2005, 53, (3), pp. 908–914.

[21] S. X. Ta, I. Park, and R. W. Ziolkowski, “Circularly polarized crossed dipole on an HIS for 2.4/5.2/5.8-GHz WLAN applications,” *IEEE Antennas Wirel. Propag. Lett.*, 2013, 12, (3), pp. 1464–1467.

[22] Y. Zhang, et al. "Planar artificial magnetic conductors and patch antennas." *IEEE Trans. Antennas Propag.*2003, 51 (10), pp. 2704-2712.

[23] Srivastava et al., "Wideband and high-gain circularly polarised microstrip antenna design using sandwiched metasurfaces and partially reflecting surface." *IET Microwaves, Antennas & Propagation*, 2018, 13, (3), pp. 305-312.

[24] Agarwal and Alphones "Triple-band compact circularly polarised stacked microstrip antenna over reactive impedance meta-surface for GPS applications." *IET Microwaves, Antennas & Propagation*, 2014, 8, (13), pp. 1057-1065

[25] L. Bernard, G. Chetier, and R. Sauleau, “Wideband circularly polarized patch antennas on reactive impedance substrates,” *IEEE Antennas Wireless Propag. Lett.*, 2011, 10, pp. 1015–1018.

[26] K. Agarwal, Nasimuddin, and A. Alphones, “RIS-based compact circularly polarized microstrip antennas,” *IEEE Trans. Antennas Propag*., 2013, 61, (2), pp. 547-554.
[27] N. Nasimuddin, Z. N. Chen, and X Qing, “Bandwidth enhancement of a single-feed circularly polarized antenna using a metasurface: metamaterial-based wideband CP rectangular microstrip antenna,” *IEEE Antennas Propagat. Mag.*, 2016, 58, (2), pp. 39-46.
[28] J. Chatterjee, A. Mohan, and V Dixit, “Broadband circularly polarized H-shaped patch antenna using reactive impedance surface,” *IEEE Antennas Wireless Propag. Lett.*, 2018, 17, (4), pp. 625-628.
[29] R. Nakamura and T. Fukusako, “Broadband design of circularly polarized microstrip patch antenna using artificial ground structure with rectangular unit cells,” *IEEE Trans. Antennas Propag.*, 2011, 59, (6), pp. 2103–2110.
[30] B. A. Austin, and K. P. Murray. “The application of characteristic-mode techniques to vehicle-mounted NVIS antennas,” *IEEE Antennas Propag. Mag.*, 1998, 40, (1), pp. 7-21.
[31] E. Newman, “Small antenna location synthesis using characteristic modes,” *IEEE Trans. Antennas Propag*., 1979, 27, (4), pp.530-531.
[32] M. Cabedo-Fabres, et al., “The theory of characteristic modes revisited: A contribution to the design of antennas for modern applications,” *IEEE Antennas Propag. Mag.*, 2007, 49, (5), pp. 52-68.
[33] Y. Chen, and C. F. Wang, “Characteristic-mode-based improvement of circularly polarized U-slot and E-shaped patch antennas,” *IEEE Antennas Wireless Propag. Lett*., 2012, 11, pp. 1474-1477.
[34] F. H. Lin, and Z. N. Chen, “Low-profile wideband metasurface antennas using characteristic mode analysis,” *IEEE Trans. Antennas Propagat.*, 2017, 65, (4), pp. 1706-1713.
[35] C. Zhao and C-F Wang, “Characteristic mode design of wide band circularly polarized patch antenna consisting of H-shaped unit cells,” *IEEE Access*, 2018, 6, pp. 25292-25299
[36] T. Li and Z. N. Chen, "A dual-band metasurface antenna using characteristic mode analysis," *IEEE Trans. Antennas Propagat.*, 2018, 66, (10), pp. 5620-5624.
[37] D. Chen, et al., “Broadband stable-gain multi-resonance antenna using non-periodic square-ring metasurface,” *IEEE Antennas Wireless Propag. Lett*., 2019, 18, 8, pp. 1537-1541.
[38] Y. Jia, Y. Liu, and S. Gong, “Slot-coupled broadband patch antenna,” *Electron. Lett*., 2015, 51, (6), pp. 445–447.
[39] N. Chamok, M. Ali, T. Anthony, and S. J. Weiss, “Ultra-thin UHF broadband antenna on a non-uniform aperiodic (NUA) metasurface”. *IEEE Antennas and Propag. Mag.*, 2015, 57, (2), pp. 167-180.
[40] L. Zhou, X. Chen, X. Duan, “Fabry–Pérot resonator antenna with high aperture efficiency using a double-layer nonuniform superstrate,” *IEEE Trans. Antennas Propag.*, 2018, 66, (4), pp. 2061-2066.
[41] C. Balanis, Antenna Theory, Analysis, and Design, 2nd ed. New York: Wiley, 1997
[42] L. I. Basilio, J. T. Williams, and D. R. Jackson, “The characterization of a slot discontinuity between two microstrip patch conductors,” in Proc. ICEAA’01, Torino, Italy, 2001, pp. 251–254.